IEEE Access
Multidisciplinary | Rapid Review | Open Access Journal

Received January 12, 2020, accepted February 8, 2020, date of publication February 12, 2020, date of current version February 25, 2020.

Digital Object Identifier 10.1109/ACCESS.2020.2973417

Manipulation of Multiple Fano Resonances Based on a Novel Chip-Scale MDM Structure

ZHENGFENG LI[1], KUNHUA WEN[1,2], LI CHEN[1], LIANG LEI[1], JINYUN ZHOU[1], DONGYUE ZHOU[1], YIHONG FANG[1], AND YUWEN QIN[2,3]

[1]School of Physics and Optoelectronic Engineering, Guangdong University of Technology, Guangzhou 510006, China
[2]Guangdong Provincial Key Laboratory of Photonics Information Technology, Guangdong University of Technology, Guangzhou 510006, China
[3]College of Information Engineering, Guangdong University of Technology, Guangzhou 510006, China

Corresponding author: Kunhua Wen (khwen@gdut.edu.cn)

This work was supported in part by the National Key Research and Development Program of China under Grant 2019YFB1803505, in part by the Science and Technology Project of Guangzhou under Grant 201904010243, in part by the Major Special Projects in Guangdong Province under Grant 2018B010114002, in part by the Program for Guangdong Introducing Innovative and Enterpreneurial Teams, and in part by the Science and Technology Planning Projects of Guangdong Province, China, under Grant 2016A020223013.

ABSTRACT A novel chip-scale metal-dielectric-metal (MDM) refractive-index sensor is proposed and investigated in this paper by using finite-difference time-domain (FDTD) method and multimode interference coupled-mode theory (MICMT), respectively. A slot cavity with an embedded tooth-shape cavity and a side-coupled semi-ring cavity are inserted between the input and output MDM waveguides. According to the simulation results, dual ultra-sharp and asymmetrical Fano peaks emerge in transmission spectrum with high performances. Besides, the transmission responses for the primary parameters of this structure are also investigated. To focus on developing integrated photonic devices, the original structure is successfully expanded by two additional semi-ring cavities through an innovative coupling approach, generating up to eight Fano peaks with outstanding characteristics. It is believed that this novel MDM structure will be a guideline for designing the chip-scale plasmonic devices.

INDEX TERMS Fano resonance, metal-dielectric-metal waveguide, plasmonic, refractive index sensing, slow light.

I. INTRODUCTION

Fano resonance, which is caused by the coherent interference between a discrete excited state and a continuum in the same energy level [1]–[4], has attracted much attention in the plasmonic fields due to its extensive application prospect in recent years. Fano resonance possesses an ultra-sharp and asymmetrical profile, which is quite different from classical Lorentz resonance. Currently, it is remarkably performing in the optical communication and optical sensing areas owing to its unique characteristics of high sensitivity (S) and high figure of merit (FOM) [5]. Meanwhile, it should be mentioned that surface plasmon polaritons (SPPs), which propagate along the metal-dielectric interface [6], have abilities to overcome the optical diffraction limit and confine light at deep subwavelength dimensions. With an acceptable propagation distance of light, nano-scale metal-dielectric-metal (MDM) structure with resonators, in which coherent interferences of SPPs will occur to generate advantageous optical phenomena, is expected as one of the most promising approaches for realizing chip-scale integrated optical circuits, and thus, various MDM devices have been proposed and investigated [7]–[12]. Consequently, considerable interest has been attracted to the MDM-based Fano resonances.

So far, single or dual Fano resonant peaks are designed and achieved in plenty of plasmonic MDM structures with several coupled cavities [10], [13]–[18]. However, due to the potential applications of Fano resonances, such as enhanced biochemical sensing [2], [19], fast light or slow light devices [3] and optical switching [20], [21], one should expect to make full use of the parallel processing capabilities of multiple Fano resonances, for developing highly integration of photonics. In this case, researchers have proposed several MDM structures to generate about three or four Fano resonances in the side-coupled systems [22], [23] or the end-coupled systems [24].

In this paper, up to eight Fano resonances are realized and investigated theoretically and numerically in a novel

The associate editor coordinating the review of this manuscript and approving it for publication was Hiram Ponce.

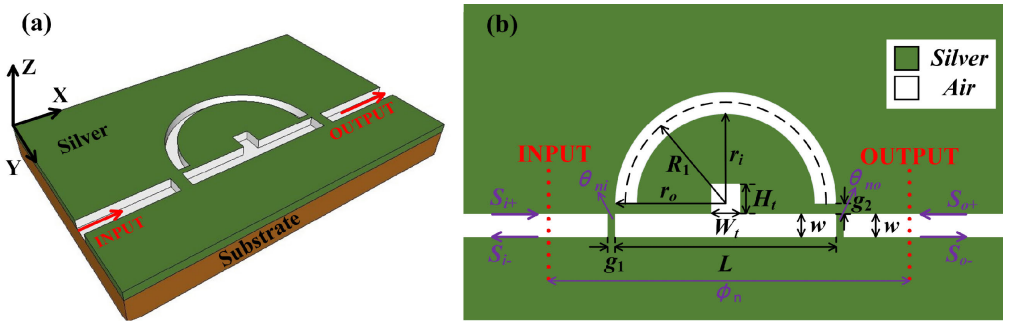

FIGURE 1. (a) 3D and (b) 2D (X-Y plane) schematic diagram of an end-coupled system composed of a slot cavity with a tooth-shape cavity and a side-coupled semi-ring cavity.

hybrid coupled system. At first, a nano-scale end-coupled system composed of a slot cavity with an embedded tooth-shape cavity and a side-coupled semi-ring cavity is proposed. By employing finite-difference time-domain (FDTD) method and multimode interference coupled mode theory (MICMT) for the proposed structure, we have investigated dual ultra-sharp and asymmetrical Fano peaks, which are attributed to the mode interactions, and these Fano peaks possess high sensitivities and high FOMs. Furthermore, multi-channel Fano resonances are successfully achieved by arranging two additional semi-ring cavities to side couple to the waveguides. This innovative coupling way and the outstanding properties of all Fano resonances are also analyzed in details. We believe that this hybrid coupled system will be a typical example for designing multi-Fano resonators in highly integrated photonic circuits.

II. STRUCTURAL MODEL AND SIMULATION ANALYSIS

The three-dimensional (3D) and two-dimensional (2D) diagrams of the proposed MDM waveguide structure are depicted in Fig. 1(a) and Fig. 1(b), respectively. An end-coupled slot cavity with a tooth-shape cavity (denoted as cavity SCT), which can be considered as a composite FP resonator holding the bright modes, is embedded between the input and output waveguides with a gap of $g_1 = 10$nm. To emerge Fano resonances, another FP resonator supporting the dark modes is required to generate the forbidden bands to interact with the pass bands of cavity SCT. Accordingly, a semi-ring cavity (denoted as cavity SR) is set to side couple to cavity SCT with a coupling distance of $g_2 = 12$nm. The center radius of cavity SR is expressed as the average of the outer and the inner radii, i.e. $R_1 = (r_o + r_i)/2$. The widths of the waveguides, the slot cavity and the semi-ring cavities are fixed as $w = 50$nm, and the length of the slot cavity is unchanged as $L = 480$nm in this paper. W_t and H_t are the width and the height of the tooth-shape cavity, respectively.

Note that at the continuous metal dielectric interface, the wave vector of SPPs is not matched with the one of incident light wave that directly injected in the input port. Therefore, in order to excite SPPs, there are several fundamental methods available for achieving wave vector matching, including prism coupling like Kretschmann method or Otto method, waveguide coupling, and grating coupling methods, and so on. The details of these approaches are not discussed in this paper because the FDTD solution software will deal with all simulations with appropriate settings.

For saving the hardware resources and the simulating time, 2D FDTD method is utilized to investigate the transmission responses of this proposed structure rather than the 3D one, since the accuracy of simulated results will not be affected. Upon Fig. 1(b), the white and green areas in this 2D model represent air ($\varepsilon_0 = 1.0$) and silver, respectively. The relative permittivity of silver ε_m is characterized by the experimental optical constant of Johnson and Christy [26]. Accordingly, the dispersion equation of SPPs propagating along the positive x direction in the MDM structure is determined by the following equation [7]:

$$\varepsilon_m k_0 \tan h\left(-\frac{jk_0 w}{2}\right) + \varepsilon_0 k_m = 0 \tag{1}$$

where w is the width of the waveguide, and $k_{0,m} = \sqrt{\varepsilon_{0,m}(2\pi/\lambda)^2 - \beta^2}$ are the transverse propagation constant in air and silver, respectively. $\beta = (2\pi/\lambda)\, n_{eff}$ is the mode propagation constant and n_{eff} is the effective refractive index. However, it is important to note that the widths of dielectric layer and the resonators are fixed as 50 nm so that only the fundamental transverse magnetic (TM_0) mode is supported in the MDM structure [7].

When SPPs are coupled into the Fabry–Pérot (FP) cavities, based on the resonant condition of a plasmonic resonator, stable standing waves can only be built up constructively at the resonant wavelengths of [26], [27]:

$$\lambda_{res} = \frac{2Re\left(n_{eff}\right) L_{eff}}{N - \varphi/2\pi}, \quad N = 1, 2, 3, \cdots \tag{2}$$

where L_{eff} is the perimeter of the cavity SCT or cavity SR, and φ is the phase shift due to the reflection on both sides of the cavity. Re $\left(n_{eff}\right)$ is the real part of the effective refractive index n_{eff} that determines the optical phase retardation of the plasmonic mode, while the imaginary part Im $\left(n_{eff}\right)$ related to the propagation loss coefficient is not considered in the calculation of resonant wavelength because it is independent with the resonant position of the interference.

When the resonant wavelength of narrow-bandwidth dark mode is close to the one of broad-bandwidth bright mode,

coherent interference between these two modes occurs because of the phase difference, leading to an asymmetrical Fano-like spectral response. According to (2), we know that the resonant wavelength is proportional to the effective length of resonator, and thus, one can generate Fano resonances by designing appropriate dimensions of resonators to control the resonant position of bright modes and dark modes. In most cases, the smaller wavelength difference between bright mode and dark mode is, the higher asymmetry of Fano resonance is. Besides, the coupling distance between resonators can also significantly affect the optical behavior of SPPs. A larger coupling distance will generally lead to a higher asymmetry but a lower transmittance of Fano resonance.

Multimode interference coupled mode theory (MICMT) [28] evolved from coupled mode theory (CMT) [29]–[31] is employed to theoretically and numerically analyze the transmission responses of the multi-Fano-based MDM structure, because MICMT performs much better than CMT in explaining asymmetric spectral phenomena. It is well known that an appropriate reference plane in the case of single mode coupling can result in zero coupling phase between the resonant mode and the waveguides, and thus, the combined field effect of the resonant modes can be considered as their field superposition. However, referring to multiple modes coupling, the fact is that the coupling phases and the moduli of different resonant modes are different and associated with each other, as well as the ones between the waveguide and each resonant mode of the resonator. Consequently, all these coupling phases and moduli will affect the entire transmission in the multi-Fano-based MDM structure. In other world, each resonant mode is generated by the weighted influences of the other modes. Thus, the results obtained by MICMT can perfectly fit the FDTD simulated curve to explain the transmission response considering all the coupling phases and moduli of the resonant modes in the interested spectral range. Accordingly, MICMT method considering the coupling phases and modulus is derived as follow [28]:

$$\begin{cases} \dfrac{\partial A_n}{\partial t} = \kappa_{ni} S_{n,i+} + \kappa_{no} S_{n,o+} - \left(j\omega_n + \dfrac{1}{\tau_n} + \dfrac{1}{\tau_{ni}} + \dfrac{1}{\tau_{no}} \right) A_n \\ S_{i-} = -S_{i+} + \sum\limits_n \kappa_{ni}^* A_n, \qquad \kappa_{ni} = \sqrt{\dfrac{2}{\tau_{ni}}} e^{j\theta_{ni}} \\ S_{o-} = -S_{o+} + \sum\limits_n \kappa_{no}^* A_n, \qquad \kappa_{no} = \sqrt{\dfrac{2}{\tau_{no}}} e^{j(\theta_{no} - \phi_n)} \\ S_{n,i+} = \gamma_{ni} e^{j\varphi_{ni}} S_{i+}, \qquad S_{n,o+} = \gamma_{no} e^{j\varphi_{no}} S_{o+}, \end{cases} \tag{3}$$

here, with respect to the *n-th* resonant mode, A_n and ω_n are the normalized amplitude and resonant frequency, respectively, τ_n denotes the decay time of internal loss resulted from the absorption and surface scattering, and $\tau_{ni,o}$ are the decay time related to the coupling between the resonator and the input/output waveguides, respectively. As schematically shown in Fig. 1(b) with purple fonts, ϕ_n describes the phase difference between the output and input ports, whereas $\theta_{ni,o}$ and $\varphi_{ni,o}$ are the coupling phases between the resonant system and the input/output waveguides, and the complex amplitude phases of the *n-th* propagating modes in input/output waveguides that will be coupled into the resonate system, respectively. $S_{i,o\pm}$ represent the amplitudes of SPPs in the input and output waveguides, respectively, whereas $S_{n,i+}$ and $S_{n,o+}$ are the normalized ones corresponding to the *n-th* resonant mode, respectively. $\gamma_{ni} e^{j\varphi_{ni}}$ and $\gamma_{no} e^{j\varphi_{no}}$ stand for the normalized coefficients, in which there is $\gamma_{\mathrm{n1}} = \gamma_{\mathrm{n2}} \approx 1$ in this paper.

Since SPPs are supposed to be launched from the input waveguide, S_{o+} equals to zero. The total effects of other resonances in uninterested spectral range can be considered as a relatively small constant $t_0 = 0.15$. Then, the complex amplitude transmission coefficient of SPPs from input waveguide to output waveguide is expressed as:

$$t = \frac{S_{o-}}{S_{i+}} = t_0 + \sum_n \frac{|\kappa_{ni}|\,|\kappa_{no}|\,e^{j\varphi_n}}{-j(\omega - \omega_n) + \frac{1}{\tau_n} + \frac{1}{\tau_{ni}} + \frac{1}{\tau_{no}}} \tag{4}$$

Besides, the input and output waveguides with identical width are symmetrically distributed with respect to cavity SCT, which results in $\tau_{ni} = \tau_{no} = \tau_{nc}$ and $\theta_{ni} = \theta_{no}$. The total phase differences of the *n-th* resonant mode are expressed as $\varphi_n = \varphi_{ni} + \phi_n + \theta_{ni} - \theta_{no} = \varphi_{ni} + \phi_n$. Thus, the transmittance of SPPs in this MDM structure can be derived as:

$$T = |t|^2 \approx \left| t_0 + \sum_n \frac{2e^{j\varphi_n}}{-j(\omega - \omega_n)\,\tau_{nc} + 2 + \frac{\tau_{nc}}{\tau_n}} \right|^2 \tag{5}$$

After setting the parameters of $R_1 = 215$nm, $W_t = 80$nm and $H_t = 75$nm, the simulated transmission spectrum and the reflection one are depicted in Fig. 2(a) using blue solid line and black dotted line, respectively. Dual symmetrical FP peaks (marked as FP1 and FP2, respectively) arise at 957 nm and 1612 nm, respectively, while dual ultra-sharp and asymmetrical Fano peaks (marked as FR1 and FR2, respectively) emerge at 703 nm and at 1083 nm, respectively. Note that for any new multi-mode structures, all resonant modes in the interested wavelength range are need to be counted for the calculation of transmittance of SPPs by the MICMT method. In this paper, all resonant modes in the same transmission spectrum are numbered from left to right, for example, FR1, FP1, FR2, and FP2 correspond to the 1th, 2nd, 3rd, and 4th resonant modes, respectively. The arguments in MICMT formulas, which are $\tau_{1c} = 120fs$, $\tau_{2c} = 30fs$, $\tau_{3c} = 130fs$, $\tau_{4c} = 60fs$, $\tau_1 = 70fs$, $\tau_2 = 70fs$, $\tau_3 = 150fs$, $\tau_4 = 55fs$, $\varphi_1 = 0.75\pi$, $\varphi_2 = 0.1\pi$, $\varphi_3 = 0.45\pi$, and $\varphi_4 = 1.85\pi$, respectively, can be obtained through curve fitting. Accordingly, the transmission response calculated by MICMT method is illustrated in Fig. 2(a) with red-circle line, which agrees well with the result simulated by FDTD method. For comparison, the spectra of the proposed structure without the tooth-shape cavity or without cavity SR are illustrated in Fig. 2(b) using blue dashed line and black dotted line, respectively. Obviously, FR1 arises from the mode interference between the dark mode of cavity SR and the bright

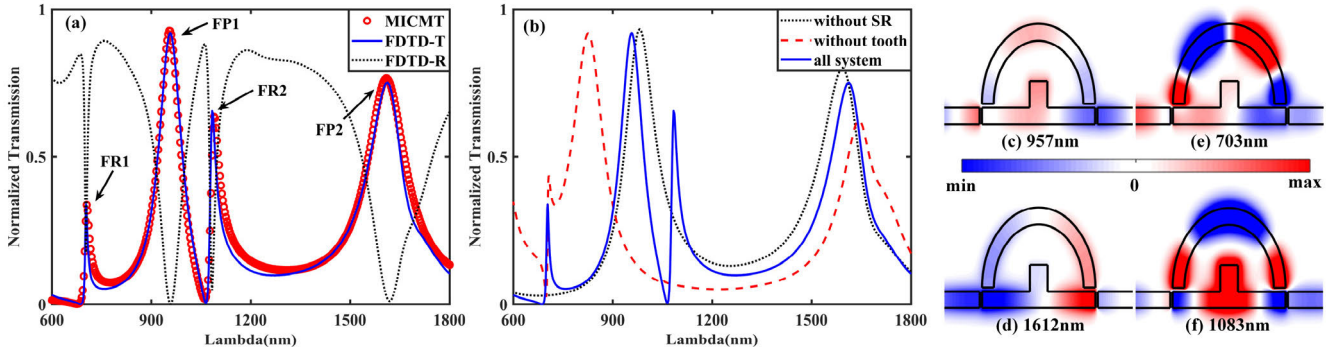

FIGURE 2. (a) The spectral responses in the proposed structure: FDTD simulated transmission response (blue solid line) and reflection response (black dotted line), and MICMT calculated transmission response (red circle line), respectively. (b) Transmission spectra of single cavity SCT, the proposed structure without tooth-shape cavity, and the whole coupled system. (c)-(f) Magnetic field distributions of resonant peaks at the wavelengths of 957nm, 1612nm, 703nm and 1083nm, respectively.

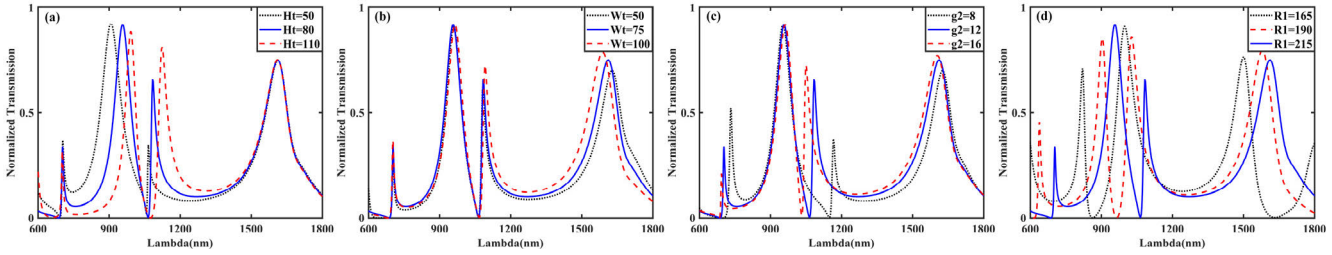

FIGURE 3. Transmission responses for the changes of the parameters of the structure: (a) height and (b) width of the tooth-shape cavity, (c) coupling distance between cavity SCT and cavity SR, (d) center radius of cavity SR.

mode of the slot cavity, whereas FR2 can be attributed to the existence of the tooth-shape cavity.

In order to excavate the underlying formation mechanism of Fano peaks, more details of magnetic field distribution at resonant peaks are shown in Figs. 2(c)-(f). From the profiles at FP peaks of 957nm and 1612nm, we can see that most of SPPs can pass through the output port of the MDM waveguide and only a few are coupled into cavity SR. At the wavelength of 703nm as shown in Fig. 2(e), SPPs are confirmed at cavity SR and both sides of the slot cavity, and an in-phase relationship exists at the joint between cavity SR and cavity SCT. Thus, FR1 is generated owing to the constructive interference between the bright mode of cavity SCT and the dark mode of cavity SR. The magnetic field distribution at the wavelength of 1083nm is depicted in Fig. 2(f), from which it is observed that SPPs are strongly concentrated inside the tooth-shape cavity. Besides, the joint between cavity SR and cavity SCT represents an anti-phase relationship, leading to the destructive interference that generates the FR2.

In this section, we will discuss the influences of the parameters of the proposed structure on transmission spectrum. Note that the resonant wavelength has proportional relationship with the dimension of resonator. Firstly, the transmission responses for different heights and widths of the tooth-shape cavity are plotted in Fig. 3(a) and Fig. 3(b), respectively. When the height H_t increases from 50nm to 110nm, the wavelengths of FR1 and FP2 are nearly unchanged, while FP1 and FR2 have a red shift. The higher tooth-shape cavity is, the more SPPs are trapped in it, resulting in enhancement of FR2, and FR1 was affected a little bit because of the multimode effect. Figure 3(b) reveals that the wavelengths of the resonant peaks move slightly, as the width W_t increases. In addition, the coupling distance between cavity SR and cavity SCT can lead to significant changes in the optical behavior of Fano resonances, as plotted in Fig. 3(c). It is observed that FP peaks remain at the same positions when g_2 increases with a step of 4 nm, because FP resonances are the interferences between the modes in cavity SCT. FR peaks arose from modes coupling have a blue shift with a penalty of transmittance for FR1 but with an enhancement for FR2. That is because the resonant wavelength of FR2 is much closer to the peak-wavelength of the corresponding bright mode, while FR1 is the opposite case. As indicated in Fig. 3(d), FR peaks will occur at different wavelengths with different parameters of cavity SR owing to the changing wavelengths of dark modes in cavity SR.

The group delay that relates to the dispersion is an important factor to develop the fast or slow light technologies for dispersion compensation management in optical fiber communication area. Fano resonance possesses positive and negative group delays simultaneously owing to its phase shifts within Fano resonant windows. The phase responses and the group delays in this MDM structure are illustrated in Fig. 4 to get an insight into Fano resonances. It is obviously observed from the blue curve that phase shifts arise around the Fano peaks at 703nm and 1083nm while opposite variations occur for the dips. This phenomenon is distinguished from the smoothly changing around the FP resonant windows. The group delays (τ) are also investigated in Fig. 4(a) using red dashed line, and it can be calculated by:

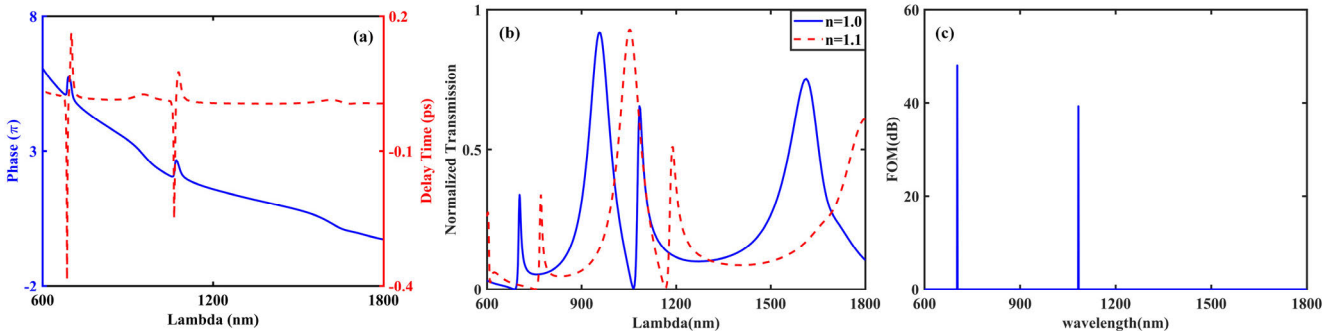

FIGURE 4. (a) Corresponding phase responses and the time delays of the proposed structure, (b) transmission responses with respect to different refractive indices, and (c) maximum FOM values of the proposed structure.

$\tau = \left(-\lambda^2 d\theta\right) / (2\pi c d\lambda)$, where θ and c denote the phase shift and the light speed, respectively. Within the Fano resonant windows, positive or negative group delays corresponding to normal dispersion or abnormal dispersion, respectively, are available around the peaks or dips, respectively. The maximums for the peaks are ∼0.16 ps and ∼0.08 ps at the wavelengths of 703nm and 1083nm, respectively, and the ones for the dips are ∼−0.39 ps and ∼−0.25 ps at the wavelengths of 686nm and 1065nm, respectively. Accordingly, these unique properties can be used to identify Fano resonances and they are also beneficial to develop the fast light or slow light technologies, such as dispersion compensation technology in optical fiber communication.

Furthermore, two more preferred factors for evaluating the sensing performances of this refractive index sensor are also investigated. One of them is the sensitivity (nm/RIU), which is defined as the resonant wavelength shift per the variation unit of refractive index, i.e. $S = \Delta\lambda_{res}/\Delta n$. As shown in Fig. 4(b), when the refractive index of the dielectric in FP cavities changes from 1.0 to 1.1, the transmission spectrum exhibits an evident red shift. Besides, the calculated sensitivities of this chip-scale sensor are 676 nm/RIU and 1062 nm/RIU for FR1 and FR2, respectively. To be more detailed for sensing applications, once the refractive index of dielectric changes as the temperature, concentration, or pressure varies, one is able to measure the shifts of the resonant peaks to calculate the refractive index variation. Thus, this proposed structure can be applied for sensing applications in different refractive index environment, such as biological and medical applications, in which the sensing materials are water-based solutions.

Another critical evaluation factor is FOM, of which a high value for Fano resonance is advantageous in sensing area. Generally, if we set a fixed wavelength at an ultra-sharp peak or an ultra-low dip, a maximum FOM value will achieve by following equation: $\text{FOM} = 10\lg\left(\max\left(\left|\partial T / \left(T\,\partial n\right)\right|\right)\right)$, where T denotes the transmittance at the specific wavelength and $\partial T/\partial n$ is the variation of transmittance at the specific wavelength due to the variation of the refractive index ∂n. Owing to the ultra-sharp asymmetrical Fano line shape, the maximum FOM values at the Fano peaks of 703 nm and 1083 nm achieve as high as ∼48.05 dB and ∼39.29 dB, respectively, as exhibited in Fig. 4(c).

III. MULTIPLE FANO RESONANCES INDUCED BY EXPANDING THE STRUCTURE

Since more and more attention have also been paid to the development of chip-scale integrated photonic circuits, it is very essential to induce more Fano resonances in single plasmonic coupled system due to their excellent parallel processing capabilities. As well known, a commonly effective approach to manipulate the channels of Fano resonances is controlling an additional cavity to couple with the original structure to lead to mode interferences between the bright modes or dark modes supported by the additional cavity and the original structure. In this paper, an innovative coupling approach is proposed to generate more Fano resonances as follows.

A. ADDING A SIDE-COUPLED SEMI-RING CAVITY ABOVE THE ORIGINAL ONE

As shown in Fig. 5(a), an additional semi-ring cavity (denoted as cavity ASR) is set above cavity SR, connecting the input and output waveguides with a coupling distance of $g_3 = 12$ nm. The center radius of cavity ASR is $R_2 = 315$ nm. Thus, the interval between cavity ASR and cavity SR is 50 nm. It means that owing to this relatively weak coupling distance, the existence of cavity ASR has only a little effect on Fano resonances in the original structure. Therefore, the transmission response and the reflection one of this expanded structure are intuitively shown in Fig. 5(b). Since a new optical path is built up, three new Fano peaks (marked as FR3, FR4, and FR5, respectively) emerge at the wavelengths of 622 nm, 753 nm, and 1480 nm, respectively. The sensitivities of three Fano peaks of FR3, FR4, and FR5 are calculated as 608 nm/RIU, 765 nm/RIU, and 1477 nm/RIU, respectively, and the corresponding maximum FOMs are 52.53 dB, 35.79 dB, and 35.99 dB, respectively. Besides, the MICMT calculated spectral response as plotted in Fig. 5(b) with the red circle line. Note that there are some deviations around the FP1 window, which is because we did not take the degenerate mode into account due to the uncertain wavelength of this uninterested mode. Even so, the MIMCT curve still have a highly consistence with the FDTD one with the blue solid line in Fig. 5(b). The MICMT values corresponding to all resonances are $\tau_1 = 70fs$, $\tau_2 = 120fs$, $\tau_3 = 70fs$, $\tau_4 = 120fs$, $\tau_5 = 140fs$, $\tau_6 = 130fs$, $\tau_7 = 70fs$,

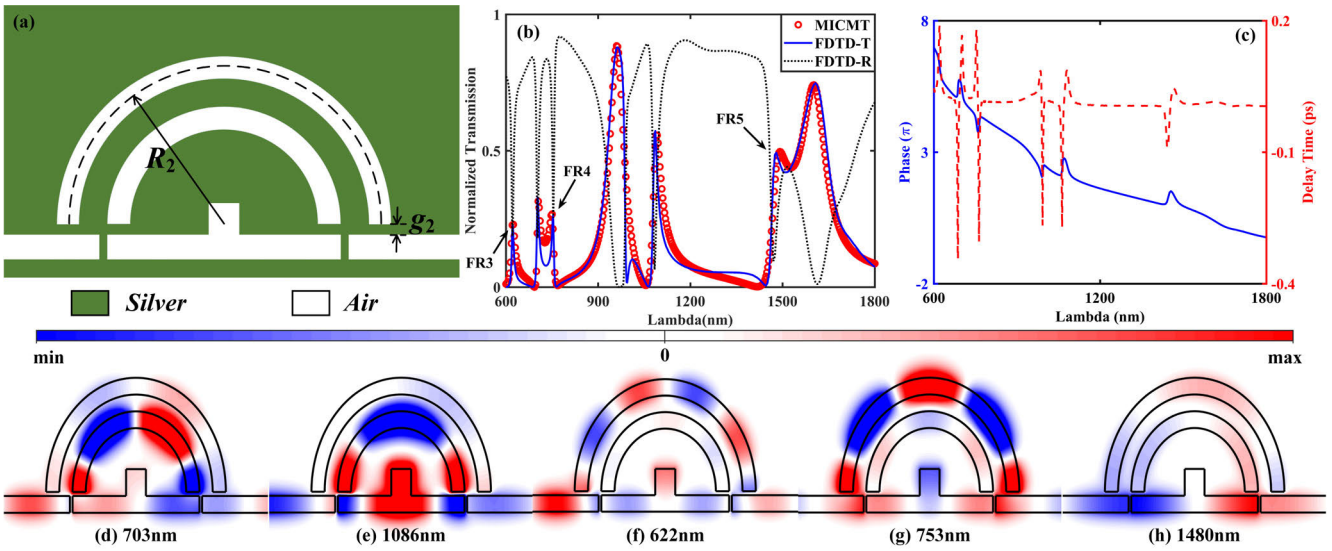

FIGURE 5. (a) Schematic diagram of the proposed structure after implementing an additional side-coupled semi-ring cavity, (b) the spectral responses in this structure: FDTD simulated transmission response (blue solid line) and reflection response (black dotted line), and MICMT calculated transmission response (red circle line), respectively, (c) variation of phase responses and group delays, and (d)-(h) magnetic field distribution of Fano peaks at the wavelengths of 703nm, 1086nm, 622nm, 753nm, and 1480nm, respectively.

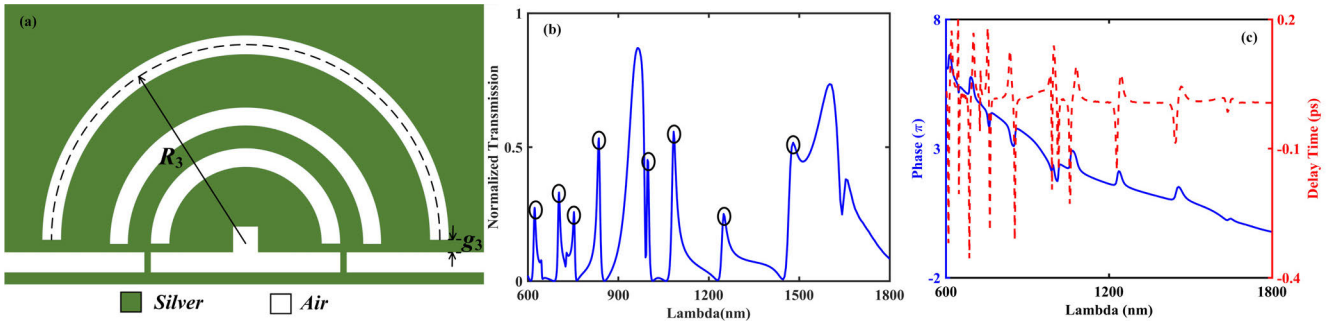

FIGURE 6. (a) Schematic diagram of the proposed structure after augmenting two semi-ring cavities. (b) Transmission responses of this hybrid system composed of two additional semi-ring cavities and the original structure. (c) Corresponding phase shifts and group delays.

$\tau_{1c} = 100fs$, $\tau_{2c} = 180fs$, $\tau_{3c} = 180fs$, $\tau_{4c} = 40fs$, $\tau_{5c} = 120fs$, $\tau_{6c} = 130fs$, $\tau_{7c} = 100fs$, $\varphi_1 = 0.9\pi$, $\varphi_2 = 0.9\pi$, $\varphi_3 = 1.75\pi$, $\varphi_4 = 0.05\pi$, $\varphi_5 = 0.35\pi$, $\varphi_6 = 0.72\pi$, $\varphi_7 = 1.95\pi$, respectively.

More details of Fano resonances are analyzed based on the phase shifts and group delays, as shown in Fig. 5(c). With similar features to Fano resonances, the phase responses of this expanded structure have an obvious shift around the Fano resonant windows, and negative or positive group delays are achieved at Fano dips or peaks. To better understand the physical phenomena of new Fano peaks, magnetic field distributions are intuitively displayed in Figs. 5(d)-(h). As shown in Fig. 5(d) and Fig. 5(e), the distributions of SPPs are the same as the ones in the original structure at peaks of FR1 and FR2, and only a few are coupled into cavity ASR. Thus, FR1 and FR2 are not influenced after adding cavity ASR. Since this proposed coupled system is a hybrid of end-coupled and side-coupled system, the coupling mechanism of SPPs is much more complex than that of the single coupled system. In this case, the end-coupled section in this structure will be considered as a defect section of the waveguides. Therefore, the complete structure is simplified as a side-coupled MDM system composed of a defect section and a side-coupled cavity ASR. As indicated in Fig. 5(f) and Fig. 5(g), few SPPs are leaked into the defect section, in which SPPs distribute at the same positions as the ones in the original structure at peak FP1, representing an in-phase and anti-phase relationship between these two cases, respectively.

Besides, most of SPPs propagate through cavity ASR to the output port. Consequently, at the wavelengths of 622 nm and 753 nm, FR3 and FR4 emerge due to the constructive and destructive interference between the bright modes of cavity ASR and the dark modes of the defect section, respectively. With respect to FR5 at 1480 nm, strong energy distributions can be observed at the defect ports and the standing wave pattern within the defect section is identical to the one of FP2 in the original structure, as shown in Fig. 5(h). Meanwhile, parts of SPPs are coupled into cavity ASR, which generates a forbidden band to constructively interact with the pass band holding by the defect section, and then,

FR5 is achieved. Accordingly, five Fano resonances with excellent performances are successfully manipulated in this novel MDM structure.

B. ADDING THE SECOND ADDITIONAL SEMI-RING CAVITY ABOVE THE CAVITY ASR

To further enhancing the integration level of optical devices, more Fano resonances generating in single plasmonic structure are preferred. Therefore, the second additional semi-ring cavity (denoted as cavity SASR) is designed above the cavity ASR with a center radius of $R_3 = 550$nm, as exhibited in Fig. 6(a). The coupling distance between cavity SASR and the waveguides is set as $g_4 = 20$nm. Figure 6(b) depicts the transmission spectrum for this multi-mode resonant system, which manipulates up to eight asymmetrical Fano peaks from the visible to the near-infrared wavelength range. The results are much better than the most of the reported ones, which are about 1-4 Fano resonant channels in single structure. The corresponding phase shifts and negative or positive delay times within the Fano resonant windows are also achieved and exhibited in Fig. 6(c). Due to the diverse applications of Fano resonances, it is believed that these outstanding characteristics in this novel plasmonic structure can be perfectly applied in chip-scale integrated optical circuits.

IV. CONCLUSION

In summary, up to eight channels of Fano resonances have been successfully realized and investigated in a novel plasmonic hybrid coupled system. Firstly, an end-coupled system is designed with dual Fano peaks at the wavelengths of 703 nm and 1083 nm, respectively. Besides, phase shifts and positive or negative group delays are investigated within the Fano resonant windows and the optimal performances of 1062 nm/RIU of sensitivity and 48.05 dB of FOM are achieved in this structure. Furthermore, the original structure is expanded in an innovative coupling approach by implementing two additional semi-ring cavities ASR and SASR. Accordingly, up to eight Fano peaks have been successfully achieved from the visible to near-infrared wavelength range. It is believed that this novel plasmonic MDM structure can be preferred in the optical communication and optical sensing areas for chip-scale integrated photonic circuits due to its innovative and instructive SPPs coupling approach.

ACKNOWLEDGMENT

The authors would like to thank the editor and the reviewers for their valuable comments and suggestions, which help improve the quality of the manuscript.

REFERENCES

[1] U. Fano, "Effects of configuration interaction on intensities and phase shifts," *Phys. Rev.*, vol. 124, no. 6, pp. 1866–1878, Dec. 1961.
[2] B. Luk'yanchuk, N. I. Zheludev, S. A. Maier, N. J. Halas, P. Nordlander, H. Giessen, and C. T. Chong, "The Fano resonance in plasmonic nanostructures and metamaterials," *Nature Mater.*, vol. 9, no. 9, pp. 707–715, Sep. 2010.
[3] A. E. Miroshnichenko, S. Flach, and Y. S. Kivshar, "Fano resonances in nanoscale structures," *Rev. Mod. Phys.*, vol. 82, no. 3, pp. 2257–2298, Aug. 2010.
[4] M. F. Limonov, M. V. Rybin, A. N. Poddubny, and Y. S. Kivshar, "Fano resonances in photonics," *Nature Photon.*, vol. 11, no. 9, pp. 543–554, Sep. 2017.
[5] J. B. Lassiter, H. Sobhani, J. A. Fan, J. Kundu, F. Capasso, P. Nordlander, and N. J. Halas, "Fano resonances in plasmonic nanoclusters: Geometrical and chemical tunability," *Nano Lett.*, vol. 10, no. 8, pp. 3184–3189, Aug. 2010.
[6] W. L. Barnes, A. Dereux, and T. W. Ebbesen, "Surface plasmon subwavelength optics," *Nature*, vol. 424, no. 6950, pp. 824–830, Aug. 2003.
[7] J. A. Dionne, L. A. Sweatlock, H. A. Atwater, and A. Polman, "Plasmon slot waveguides: Towards chip-scale propagation with subwavelength-scale localization," *Phys. Rev. B, Condens. Matter*, vol. 73, no. 3, Jan. 2006, Art. no. 035407.
[8] X. Luo, X. Zou, X. Li, Z. Zhou, W. Pan, L. Yan, and K. Wen, "High-uniformity multichannel plasmonic filter using linearly lengthened insulators in metal–insulator–metal waveguide," *Opt. Lett.*, vol. 38, no. 9, pp. 1585–1587, May 2013.
[9] F. Galvez, J. Del Valle, A. Gomez, M. R. Osorio, D. Granados, D. Pérez De Lara, M. A. García, and J. L. Vicent, "Plasmonic nanodevice with magnetic funcionalities: Fabrication and characterization," *Opt. Mater. Express*, vol. 6, no. 10, p. 3086, Oct. 2016.
[10] K. Wen, Y. Hu, L. Chen, J. Zhou, L. Lei, and Z. Guo, "Fano resonance with ultra-high figure of merits based on plasmonic metal-insulator-metal waveguide," *Plasmonics*, vol. 10, no. 1, pp. 27–32, Feb. 2015.
[11] G. Wang, A. Shen, C. Zhao, L. Yang, T. Dai, Y. Wang, Y. Li, X. Jiang, and J. Yang, "Fano-resonance-based ultra-high-resolution ratio-metric wavelength monitor on silicon," *Opt. Lett.*, vol. 41, no. 3, pp. 544–547, Feb. 2016.
[12] K. Wen, Y. Hu, J. Zhou, L. Lei, J. Li, and Y. Wu, "Plasmonic-induced absorption in an end-coupled metal-insulator-metal resonator structure," *Opt. Mater. Express*, vol. 7, no. 2, pp. 433–443, Feb. 2017.
[13] J. J. Chen, Z. Li, J. Li, and Q. H. Gong, "Compact and high-resolution plasmonic wavelength demultiplexers based on Fano interference," *Opt. Express*, vol. 19, no. 10, pp. 9976–9985, Sep. 2011.
[14] X. J. Piao, S. Yu, S. Koo, K. Lee, and N. Park, "Fano-type spectral asymmetry and its control for plasmonic metal-insulator-metal stub structures," *Opt. Express*, vol. 19, no. 11, pp. 10907–10912, May 2011.
[15] J. W. Qi, Z. Q. Chen, J. Chen, Y. D. Li, W. Qiang, J. J. Xu, and Q. Sun, "Independently tunable double Fano resonances in asymmetric MIM waveguide structure," *Opt. Express*, vol. 22, no. 12, pp. 14688–14695, Jun. 2014.
[16] J. J. Chen, C. W. Sun, and Q. H. Gong, "Fano resonances in a single defect nanocavity coupled with a plasmonic waveguide," *Opt. Lett.*, vol. 39, no. 1, pp. 52–55, Jan. 2014.
[17] Z. Chen, L. Yu, L. L. Wang, G. Y. Duan, Y. F. Zhao, and J. Xiao, "Sharp asymmetric line shapes in a plasmonic waveguide system and its application in nanosensor," *J. Lightw. Technol.*, vol. 33, no. 15, pp. 3250–3253, 2015.
[18] Z. Chen, J. Chen, L. Yu, and J. Xiao, "Sharp trapped resonances by exciting the anti-symmetric waveguide mode in a metal-insulator-metal resonator," *Plasmonics*, vol. 10, no. 1, pp. 131–137, Feb. 2015.
[19] H. Lu, X. M. Liu, D. Mao, and G. X. Wang, "Plasmonic nanosensor based on Fano resonance in waveguide-coupled resonators," *Opt. Lett.*, vol. 37, no. 18, pp. 3780–3782, Sep. 2012.
[20] H. Lu, X. Liu, L. Wang, Y. Gong, and D. Mao, "Ultrafast all-optical switching in nanoplasmonic waveguide with Kerr nonlinear resonator," *Opt. Express*, vol. 19, no. 4, p. 2910, Feb. 2011.
[21] M. Heuck, P. T. Kristensen, Y. Elesin, and J. Mork, "Improved switching using Fano resonances in photonic crystal structures," *Opt. Lett.*, vol. 38, no. 14, pp. 2466–2468, Jul. 2013.
[22] Z. Chen, X. K. Song, G. Y. Duan, L. L. Wang, and L. Yu, "Multiple Fano resonances control in MIM side-coupled cavities systems," *IEEE Photon. J.*, vol. 7, no. 3, Jun. 2015, Art. no. 2701009.
[23] Z. C. Guo, K. H. Wen, Q. Y. Hu, W. H. Lai, J. Y. Lin, and Y. H. Fang, "Plasmonic multichannel refractive index sensor based on subwavelength tangent-ring metal-insulator-metal waveguide," *Sensors*, vol. 18, no. 5, May 2018, Art. no. 1348.
[24] K. H. Wen, L. Chen, J. Y. Zhou, L. Lei, and Y. H. Fang, "A plasmonic chip-scale refractive index sensor design based on multiple Fano resonances," *Sensors*, vol. 18, no. 10, Oct. 2018, Art. no. 3181.
[25] P. B. Johnson and R. W. Christy, "Optical constants of the noble metals," *Phys. Rev. B, Condens. Matter*, vol. 6, no. 12, pp. 4370–4379, Jul. 2002.

[26] Q. Zhang, X. G. Huang, X. S. Lin, J. Tao, and X. P. Jin, "A subwavelength coupler-type MIM optical filter," *Opt. Express*, vol. 17, no. 9, pp. 7549–7555, Apr. 2009.
[27] F. F. Hu, H. X. Yi, and Z. P. Zhou, "Band-pass plasmonic slot filter with band selection and spectrally splitting capabilities," *Opt. Express*, vol. 19, no. 6, pp. 4848–4855, Mar. 2011.
[28] S. L. Li, Y. L. Wang, R. Z. Jiao, L. L. Wang, G. Y. Duan, and L. Yu, "Fano resonances based on multimode and degenerate mode interference in plasmonic resonator system," *Opt. Express*, vol. 25, no. 4, pp. 3525–3533, Feb. 2017.
[29] H. Haus and W. P. Huang, "Coupled-mode theory," *Proc. IEEE*, vol. 79, no. 10, pp. 1505–1518, Oct. 1991.
[30] B. E. Little, S. T. Chu, H. A. Haus, J. Foresi, and J.-P. Laine, "Microring resonator channel dropping filters," *J. Lightw. Technol.*, vol. 15, no. 6, pp. 998–1005, Jun. 1997.
[31] C. Manolatou, M. J. Khan, S. Fan, P. R. Villeneuve, H. A. Haus, and J. D. Joannopoulos, "Coupling of modes analysis of resonant channel add-drop filters," *IEEE J. Quantum Electron.*, vol. 35, no. 9, pp. 1322–1331, Sep. 1999.

ZHENGFENG LI received the bachelor's degree from the Guangdong University of Technology, Guangzhou, China, in 2018, where he is currently pursuing the Ph.D. degree. His current interest includes nano-optics and surface plasmon polaritons.

KUNHUA WEN received the B.E. and Ph.D. degrees from Southwest Jiaotong University, Chengdu, China, in 2007 and 2013, respectively. He is currently an Associate Professor with the Guangdong University of Technology, Guangzhou, China. He is the author or coauthor of more than 50 articles published in distinguished peer-reviewed journals. His current research interests include nano-photonics, optical sensing, and optical fiber Bragg grating.

LI CHEN received the bachelor's degree in physics and the master's degree in optics from South China Normal University, Guangzhou, Guangdong, China, in 1987 and 1990, respectively. She is currently a Professor with the School of Physics and Optoelectronic Engineering, Guangdong University of Technology, Guangzhou, China. Her research interests include the optical information processing, optical design, laser biology, and laser spectroscopy.

LIANG LEI received the bachelor's degree in physics, the master's degree in optics, and the Ph.D. degree in optics from Sun Yat-sen University, Guangzhou, Guangdong, China, in 2002, 2004, and 2007, respectively. He is currently a Professor with the School of Physics and Optoelectronic Engineering, Guangdong University of Technology, Guangzhou. His research interests include the photoelectric vision detection, ultraviolet laser lithography, and ultrafast high-energy laser processing

JINYUN ZHOU received the bachelor's degree from Henan University, Kaifeng, Henan, China, in 1985, and the Ph.D. degree in optics from the Anhui Institute of Optics and Mechanics, Chinese Academy of Sciences, Hefei, Anhui, in 1997. He is currently a Professor with the School of Physics and Optoelectronic Engineering, Guangdong University of Technology, Guangzhou, China. His research interests include photo-lithography, optomechatronics, and laser technology.

DONGYUE ZHOU was born in Hunan, China. He received the M.S. degree in optics and the Ph.D. degree in electromagnetic field and microwave technology from South China Normal University, Guangzhou, China, in 2003 and 2015, respectively. From 2018 to 2019, he was a Visiting Scholar with the Department of Electronic Engineering, Southwest Jiaotong University, Chengdu, China. He is currently a Lecturer with the Guangdong University of Technology. His current research interests include optical communication, microwave photonics, wireless communications, and signal processing.

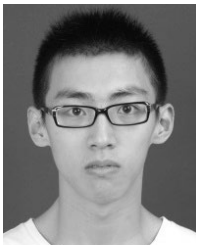

YIHONG FANG received the bachelor's degree from the Guangdong University of Technology, Guangzhou, China, in 2017, where he is currently pursuing the Ph.D. degree. His current interest involves nano-optics and surface plasmon polaritons.

YUWEN QIN received the M.S. degree from the Chinese Academy of Sciences, Xi'an, China, in 1992, and the Ph.D. degree from Tianjin University, Tianjin, China, in 1996. He is currently a Professor with the College of Information Engineering, Guangdong University of Technology, Guangzhou, China. He has been paying close attention to the research work of frontier foundation and applied foundation of information science, especially the research work of optical fiber communication and optical fiber sensing.